THE JOURNAL OF PHYSICAL CHEMISTRY A
A JOURNAL OF THE AMERICAN CHEMICAL SOCIETY

pubs.acs.org/JPCA

Article

The Potential Energy Profile of the HBr^+ + HCl Bimolecular Collision

Kazuumi Fujioka, Karl-Michael Weitzel, and Rui Sun*

Cite This: *J. Phys. Chem. A* 2022, 126, 1465−1474

Read Online

ACCESS | Metrics & More | Article Recommendations | Supporting Information

ABSTRACT: Recently, the HBr^+ + HCl bimolecular reaction has been exploited by guided ion beam studies to probe the effect of rotational excitations and collision energies on the dynamics of the ion−molecule reactions. The current manuscript employs high-level *ab initio* calculations and reports the potential energy of pathways leading to various products, including HBr + HCl^+, H_2Cl^+ + Br, H_2Br^+ + Cl, and H_2 + $BrCl^+$. The study shows that the intermediates involved in this reaction are connected by low-lying transition states, thus frequent isomerizations and diverse products are expected. Further, this manuscript screens the performance of 192 different combinations of computationally efficient methods and basis sets in order to identify the optimal quantum chemical method for further dynamics simulations.

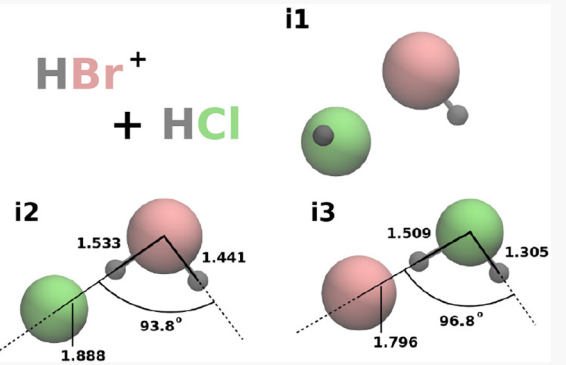

1. INTRODUCTION

Chemical reaction is a process of excess energy of the reaction system localizing into a certain vibration mode to break the chemical bond. Therefore, the way that the system is excited has a profound impact on how the reaction proceeds. For example, the well-established "Polanyi rules", proposed by John Polanyi in 1972, state that increasing the vibrational energy of the reactants is more efficient than the translational energy (i.e., collision excitation) in promoting bimolecular collision with a "late-barrier", which is defined as a transition state (TS) that closely resembles the products instead of the reactants.[1−6] In regard to the impact of the rotational energy of the reactants, it is less chemically intuitive and has only been sparsely investigated. In a pioneering study by Viggiano et al., rotational excitation has been attributed to have a similar impact as the translational excitation in endothermic reactions, while for exothermic reactions, rotational excitation has a large impact only when one or both of the reactants have a large rotational constant.[7] However, this statement is put into question by more studies of various reaction systems.[8−10]

As such, a better understanding of the rotational excitation could shed light on predicting and controlling the outcome of a reaction. Assuming single-collision conditions, simple, elementary reactions in the gas phase are ideal prototypes for such studies. Weitzel et al. have conducted a series of ion−molecule beam experiments to investigate the impact of various excitations on the dynamics of chemical reactions.[11−14] For example, the collision of HBr^+ + HBr could form Br + H_2Br^+ through proton transfer (PT) and hydrogen abstraction (HA) or HBr + HBr^+ through charge transfer (CT) and hydrogen exchange (HE).[14] It has been reported that as the rotational energy increases, the combined PT/HA reactivity monotonically decreases, while the combined CT/HE reactivity increases.[14] However, the impact of the rotational energy is quite different in a similar reaction, HCl^+ + HCl, whose PT/HA reactivity demonstrates a local minimum.[13] An *ab initio* molecular dynamics (AIMD) simulation of this reaction unraveled the mechanism: The fine balance between translational motion, rotational motion, and intermolecular interaction determines the distribution of the orientation between the reactant molecules at the moment of the collision, which governs the reactivity of the reaction.[15]

Although both reactions report that the impact of the rotational energy is more profound when the total energy in the system is low, the nature of the impact has been shown to be different even for very similar reaction systems. One difficulty associated with these reactions is to distinguish reaction pathways of the same mass-spectrometry signal. For example, the PT and HA pathways (forming H_2Cl^+ + Cl) could not be individually measured even with H/D isotopes.[13] For this reason, bimolecular collisions of HBr^+ + HCl are conducted, which will not only distinguish all reaction pathways but could also shed light on the nature of the impact of rotational energy.

This manuscript studies the potential energy profile of the HBr^+ + HCl bimolecular collision with two objectives: (1) accurately characterize the intermediates, TSs, and products involved in this reaction with state of the art *ab initio* calculations and (2) identify a computationally efficient

Received: September 20, 2021
Revised: February 11, 2022
Published: February 23, 2022

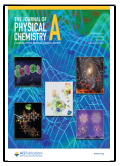

https://doi.org/10.1021/acs.jpca.1c08300
J. Phys. Chem. A 2022, 126, 1465−1474

quantum chemistry method that is suitable for future AIMD simulations. As shown in the manuscript, this seemingly simple bimolecular collision leads to a fairly large number of products through various reaction pathways. Although objective (1) is nondiscriminative with respect to potential energy, for objective (2), since the impact of the rotational energy is most profound when the total energy of the system is small, the focus is on the intermediates, TSs, and products that are energetically accessible (defined later). Under such conditions, a few products are expected such as HBr + HCl^+, Cl + H_2Br^+, and Br + H_2Cl^+, which have seen a fair amount of study,[13,14,16] as well as another set of products: H_2 + $BrCl^+$. The latter only has literature focused on its photodissociation and spectroscopy.[17−19] The only possible products excluded in this study due to high potential energy are the unstable protonated dihalogens, namely H + $HClBr^+$ and H + $HBrCl^+$, for which only analogous species (HCl_2^+, HBr_2^+, $HFCl^+$) have had very limited experimental study.[20,21]

2. METHODS

2.1. Benchmark Potential Energy Profile. Although there have been studies of the potential energy profiles of the HBr^+ + HBr and HCl^+ + HCl bimolecular collisions,[15,22] there has been no such information reported for the HBr^+ + HCl system. To balance computational cost and accuracy, coupled cluster with single and double excitations and perturbative triples (CCSD(T))[23] with cc-pVDZ[24] are used to optimize the critical points, including intermediates, TSs, and products, of this reaction. CCSD(T) includes a select number of triple excitations in the Hamiltonian to better account for the electron correlation. The optimization of the products is also performed with CCSD(T)/cc-pVTZ,[24] and their structures are compared with the experimental values. Table S1 in the Supporting Information summarizes these results: The gain in accuracy in molecular structures by moving up from double-ζ to triple-ζ is marginal, while the computational cost increases considerably. Therefore, CCSD(T) with cc-pVDZ is selected to search for and optimize the critical points of this reaction, whose geometry is used for single point energies calculation with cc-pVDZ, cc-pVTZ, and cc-pVQZ. As these energies successively become lower, they can be extrapolated to their complete basis set (CBS) limit.[25−27] CCSD(T)/CBS, by mimicking *ab initio* calculations with basis sets of infinite size, is considered one of the most trustworthy benchmarks that are theoretically achievable.

Intermediates, products, and TSs predicted by CCSD(T)/cc-pVDZ are confirmed to have the correct number and type of normal modes with their frequency calculations (i.e., $3N - 6$ nonzero frequencies for nonlinear molecules, $3N - 5$ nonzero frequencies for linear molecules, and 1 imaginary frequency for TS; N is the number of atoms in the molecule). The connections between TSs and intermediates are further confirmed by checking their intrinsic reaction coordinate (IRC)[28−30] and/or nudged elastic band (NEB).[31] Although unlikely to be traversed during a trajectory in molecular dynamics simulations, the IRC represents the vibration-less, rotation-less path connecting intermediates and can be thought of as the idealized reaction coordinate. Finally, CCSD(T)/cc-pVDZ zero-point energy (ZPE), scaled with an anharmonic scaling factor of 0.963,[32] is added to the CCSD(T)/cc-pVDZ//CCSD(T)/CBS potential. All calculations were done with NWChem version 6.8.[33]

The energetics computed from the aforementioned method (i.e., CCSD(T)/cc-pVDZ// CCSD(T)/CBS) are verified with experimental heats of reaction when available (i.e., all the products). It is important to acknowledge that the energy computed with the aforementioned method does not take into account the spin−orbit (SO) coupling effect of the system (thus referred to as "spin-free" in this manuscript). However, the positively charged diatomics ($BrCl^+$, HBr^+, and HCl^+) and neutral monatomics halogens (Br and Cl) are all open-shell molecules containing heavy atoms which could exhibit non-negligible SO coupling effect. Therefore, the experimental heat of formation, measured at a specific SO coupling state, should be properly shifted to a spin-free energy before comparing against energies calculated from CCSD(T)/cc-pVDZ//CCSD(T)/CBS.[34,35] For the charged diatomics, four degenerate spin-free $^2\Pi$ states split into a double-degenerate $^2\Pi_{3/2}$ and double-degenerate $^2\Pi_{1/2}$ state. For the monatomics, six degenerate spin-free ^2P spin states split into a quadruple-degenerate $^2P_{3/2}$ state and double-degenerate $^2P_{1/2}$ state. Therefore, with this 1:1 and 2:1 ratio of splitting between the ground SO and excited SO states, the spin-free energy is calculated, as shown in Figure S1 in the Supporting Information. This approach has been applied in previous studies and provided a fair comparison to experimental results.[36−38] The potential energy profile computed from CCSD(T)/cc-pVDZ//CCSD(T)/CBS serves as the benchmark for selecting a computationally efficient method for *ab initio* molecular dynamics simulations.

2.2. Computationally Efficient Method for *ab initio* Molecular Dynamics Simulations. In AIMD simulations, the position of the atoms is propagated according to classical equations of motion with the force (i.e., energy gradients) computed with quantum chemistry methods. Due to the enormous amount of energy gradient calculations demanded by AIMD simulations (usually on the orders of millions), the quantum chemistry method employed has to be computationally efficient and accurately represent the potential energy of the system. As noted in the previous section, the impact of the rotational excitation is most profound when the excess energy in the system is low. Therefore, the future AIMD simulation will employ a relative translational energy of 19.3−33.8 kJ/mol (0.20−0.35 eV) and a rotational energy of 0−4.8 kJ/mol (0−0.05 eV). Combining these energies with the vibrational energy (∼33.1 kJ/mol) of the reagents under experimental conditions, a cutoff energy of 100 kJ/mol (above the separated reagents) is employed to select energetically accessible structures with the CCSD(T)/cc-pVDZ//CCSD(T)/CBS level of theory for this reaction. In other words, even if certain structures of more than 100 kJ/mol above the reagents are characterized by CCSD(T)/cc-pVDZ//CCSD(T)/CBS, they would be left out as part of the benchmark in selecting a computationally efficient method for AIMD simulations. Eight commonly used methods (MP2,[39] MP2 with the frozen core approximation (FC-MP2),[39] B3LYP,[40] Becke97,[41] Becke98,[42] PBE0,[43] BNL,[44] and CAM-B3LYP[45]) coupled with 24 different combinations of basis sets (6-311G**,[46] 6-31G**,[47] 6-311G*,[46] 6-31G*,[47] aug-cc-pVDZ,[48] aug-cc-pVTZ,[48] cc-pVDZ,[24] cc-pVTZ,[24] def2-SVP,[49] def2-SVPD,[50] aug-pc-0,[51] pc-0,[51] def2-TZVP,[49] def2-TZVPD,[50] aug-pc-1,[51] aug-pc-2,[51] pc-1,[51] pc-2,[51] Sapporo-DZP-2012,[52] Sapporo-DZP-2012-diffuse[52]) and two effective core potentials (ECPs) (LAN2DZ,[53] LAN2DZdp[54]) are screened. Each method/basis set/ECP combination attempts to locate the noted critical points on the benchmark potential

https://doi.org/10.1021/acs.jpca.1c08300
J. Phys. Chem. A 2022, 126, 1465−1474

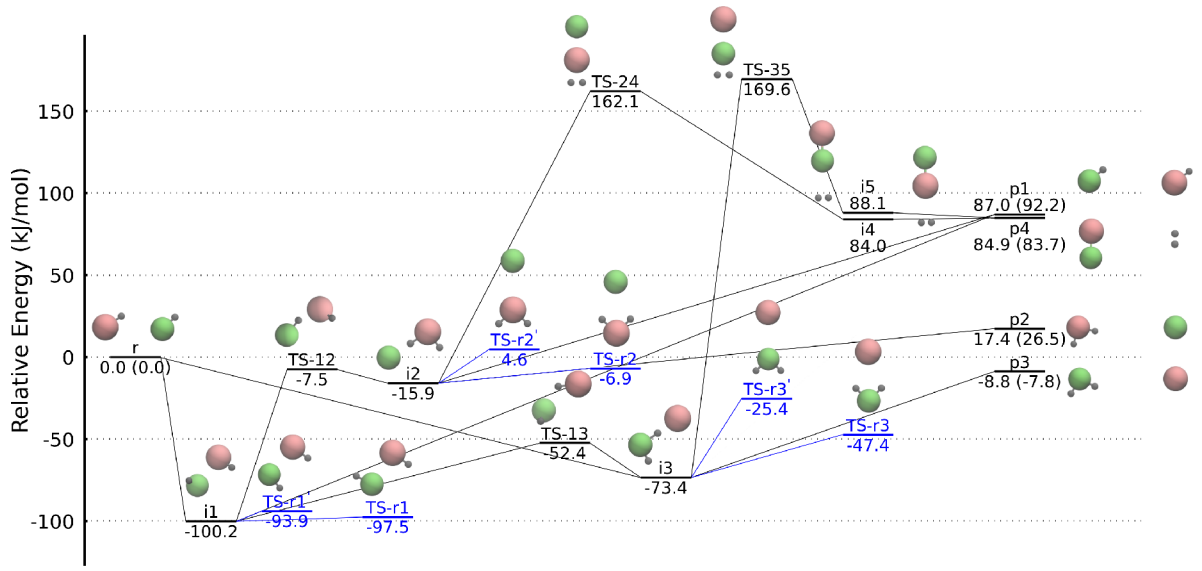

Figure 1. The potential energy profile of the HBr^+ + HCl bimolecular collision (reactants "r", products "p", intermediates "i", and transition states "TS"). For each product, the formal positive charge is located on the molecule on the left, that is, HCl^+, $BrCl^+$, H_2Br^+, and H_2Cl^+ for **p1**, **p4**, **p2**, and **p3**, respectively. The energies are computed at the CCSD(T)/cc-pVDZ//CCSD(T)/CBS level of theory. ZPEs, computed at CCSD(T)/cc-pVDZ and scaled by 0.963 for anharmonicity, are included (see section 2.1). The energies in parentheses are experimental values. Rotation pathways are colored blue. Atoms colored pink, light green, and gray are bromine, chlorine, and hydrogen, respectively.

energy profile. The performance of the AIMD candidate method is assessed by its ability to reproduce the benchmark potential energy profile and the computation cost. This protocol of selecting a quantum chemistry method for AIMD simulations has been widely used and has seen great success in elaborating experimental discoveries (please see the Supporting Information for examples).[15,36,37,55,56]

3. RESULTS

3.1. Heat of the Reaction. It is important to confirm the validity of the benchmark *ab initio* method, CCSD(T)/cc-pVDZ//CCSD(T)/CBS, with experiments when available, for example, experimental heats of reaction. Bimolecular products as a result of the HBr^+ + HCl collision are depicted in Figure 1. The heats of the reaction can be calculated from the stoichiometrically weighted sums of heats of formation of the reactants minus the stoichiometrically weighted sums of heats of formation of the products. The heats of reaction for each reaction channel (**p1**, HBr + HCl^+; **p2**, H_2Br^+ + Cl; **p3**, H_2Cl^+ + Br; **p4**, $BrCl^+$ + H_2) is compared with experimental heats of reaction at 0 K,[32,57] which is summarized in Table S2 in the Supporting Information.

As explained in section 2.1, the heats of formation of the molecules with unpaired electrons are measured at the SO ground state, thus should be shifted accordingly to get the spin-free energy to compare against the energies computed with CCSD(T)/cc-pVDZ//CCSD(T)/CBS. The SO splitting constant of the molecules involved is obtained from various spectroscopy studies[17,58] and summarized in Table S3 in the Supporting Information. It is important to note that since there is a net positive charge in the bimolecular products, at least in theory, the positive charge could be observed on either molecule. However, the listed products do not include unstable species that must lead to further dissociations. For example, since neutral H_2Cl (H_2Br) is the saddle point for the reaction H + HCl → HCl + H (H + HBr → HBr + H), the product H_2Cl + Cl^+ (H_2Br + Br^+) is not included. As Figure 1 demonstrates, the benchmark *ab initio* method, CCSD(T)/cc-pVDZ//CCSD(T)/CBS, shows excellent agreement with the experimental heats of reaction. For the four energetically accessible products (i.e., heats of reaction <100 kJ/mol, see section 2.2), **p1**−**p4**, all of their CCSD(T)/cc-pVDZ//CCSD(T)/CBS heats of reaction are within 10 kJ/mol of the experimental values, and two (**p3** and **p4**) are even within 2 kJ/mol. This level of accuracy indicates that CCSD(T)/cc-pVDZ//CCSD(T)/CBS is able to produce a reliable theoretical characterization of the HBr^+ + HCl bimolecular collision. Therefore, it is employed as the benchmark to search for the intermediates and TSs that are involved in the pathways of forming **p1**−**p4**.

3.2. Potential Energy Profile. All intermediates and TSs involved in pathways leading to **p1**, **p2**, **p3**, or **p4** are depicted in Figure 1. We note that the real dynamics of a chemical reaction does not strictly follow the IRC, nonetheless, analyzing the potential energy profile of the reaction sheds light on the possible mechanisms involved. There are two entrance channels for this reaction. The first one is facilitated by the interactions between the halogens (Cl and Br) and leads to **i1**. The second one (**i3**) is a result of HBr^+ shuffling its H to the Cl of the HCl molecule. These two intermediates are connected through a TS, **TS-13**, and the transition path from **i1** and **i3** is submerged (relative energy of the path is less than the separated reagents). The **i1** entrance channel forks into three different routes. The first one is to directly dissociate to **p1** (HBr + HCl^+), following the **r** → **i1** → **p1** pathway. For the second route, **i1** traverses through a transition state **TS-13** to isomerize to **i3**, which either directly dissociates to **p3** (H_2Cl^+ + Br), following the submerged **r** → **i1** → **TS-13** → **i3** → **p3** pathway, or overcomes a reaction barrier (**TS-35**) to isomerize to **i5** before dissociating to **p4** ($BrCl^+$ + H_2), following the **r** → **i1** → **TS-13** → **i3** → **TS-35** → **i5** → **p4** pathway. The third route that stems from the **i1** entrance channel involves the isomerization to **i2** through **TS-12**, followed by either a direct dissociation to **p1** (i.e., **r** → **i1** → **TS-12** → **i2** → **p1**) or to **p4**

https://doi.org/10.1021/acs.jpca.1c08300
J. Phys. Chem. A 2022, 126, 1465−1474

via postreaction complex **i4** (i.e., **r** → **i1** → **TS-12** → **i2** → **TS-24** → **i4** → **p4**). In regard to the **i3** entrance channel, it could isomerize to **i1** through **TS-13**, which will then populate all the aforementioned pathways. The other routes of the **i3** entrance channel include a submerged **r** → **i3** → **p3** (direct dissociation of **i3**) pathway and a classic ion-molecular double-well **r** → **i3** → **TS-35** → **i5** → **p4** pathway. Through the analysis of these reaction pathways, it is obvious that although the relative energy of **p4** is only 84.9 kJ/mol above the separated reagents, the only two pathways of forming **p4**, either through **TS-24** (and **i4**) or **TS-35** (and **i5**) are forbidden under the condition of low excess energy; **TS-24** (162.1 kJ/mol) and **TS-35** (169.6 kJ/mol) are well above the 100 kJ/mol energy cutoff criterion that is relevant to the dynamics study of the rotational excitation (see section 1 for more information). As a result, **TS-24**, **TS-34**, **i4**, **i5**, and **p4** are not further discussed in this manuscript or included in the benchmark potential energy profile to select the computationally efficient method for AIMD simulations.

The potential energy profile of the HBr^+ + HCl bimolecular collision also highlights the TSs that are related to the intramolecular twist of the system. As shown in Figure 1, each of the energetically accessible intermediates (**i1**, **i2**, **i3**) can traverse through two TSs (colored in blue) and convert back to themselves. This configuration change is further detailed in Figure 2. As shown in the bottom panel, the rotation of HBr with respect to the Cl−Br axis is almost barrierless: **TS-r1** and **TS-r1′** are only 2.7 and 6.3 kJ/mol above **i1**, respectively.

The rotation of Cl around H_2Br^+ (middle panel) is against slightly higher barriers − a full rotation involving crossing the 9.0 kJ/mol **TS-r2** and then the 20.5 kJ/mol **TS-r2′** (energies are relative to **i2**). Starting from the **i3** intermediate, the barriers involved in the rotation of Br around H_2Cl are the highest, including **TS-r3** of 26.0 kJ/mol and **TS-r3′** of 48.0 kJ/mol (energies are relative to **i3**). Here we reiterate that the connections between these TSs and their corresponding intermediates are carefully confirmed with IRC calculations. It is also important to note the potential impact of the "rotational" TSs related to **i2** and **i3** on the products. They give the opportunity of shuffling two H atoms in the reaction system, which will determine the source of the H atom in the HCl^+ cation of **p1**. For example, if we denote H(1) as the atom initially in HBr^+ and H(2) as the atom initially in HCl, H(1) would be the atom between Br and Cl in **i3**, which is formed immediately after the collision. However, after experiencing the rotation of the Br through **TS-r3** and/or **TS-r3′**, H(2) could be shuffled to be between Br and Cl in **i3**, which then goes through isomerization to **i1** before dissociating to **p1**. Depending on the number of crossings of these two TSs, the H atom in the HCl^+ cation of **p1** could be either H(1), deemed as the HE product, or H(2), deemed as the CT product. Since all these barriers are relatively low in potential energy (e.g., on the level of or lower than the separated reagents), it is expected that the configurations depicted in Figure 2 are frequently involved in the dynamics of this reaction. Indeed, the shuffling of H atoms has been observed in a similar reaction of HCl^+ + HCl, when the cation of the reagents is deuterium labeled, with the guided beam experiment[13] as well as AIMD simulations.[15] Another interesting aspect of the potential energy profile of the HBr^+ + HCl bimolecular collision is the absence of the **i2** entrance channel. Here, we reiterate that the real dynamics of a chemical reaction does not necessarily follow the aforementioned pathways, nonetheless, two structures on the potential energy profile are connected (see Figure 1 and Figure 2) if the association between them is without a potential barrier (i.e., TS). As discussed in section 2.1, the connections between intermediates and TSs in this study are confirmed with the well-adopted IRC and/or NEB method. However, when it comes to assigning the potential connection between an intermediate and separated molecules (e.g., the potential connection between **p1** and **i2**), since there is not a normal mode of imaginary frequency to follow (e.g., as in the case of IRC), a steepest energy descent algorithm is employed. Take the potential connection between **p1** and **i2** as an example again, the algorithm works as the following: The separated molecules (**p1**, HBr, and HCl^+ are separated by ∼10 Å) are aligned to resemble the target intermediate (**i2**). The energy gradient is calculated, and the configuration of the system is updated by following the descent of the energy gradient with a fine geometrical displacement (maximum displacement of any single atom is 0.16 Å). From a different perspective, this algorithm is a dynamic simulation of an infinitesimal time step with the initial velocity of atoms set to zero, and the velocity of atoms at each step (i.e., geometry update) set to zero as well. The algorithm stops when the geometry is numerically converged, indicating that a potential energy minimum has been reached. If the association between separated molecules is barrierless, *both* the potential energy of the system and the distance between the two separated molecules should monotonically decrease with the number of geometry updates until the system converges to the target intermediate. This is the case for **r**-**i3** and **p1**-**i2**, which are depicted in the top row of Figure 3. In regard to the association between **r**-**i2** and **p1**-**i3**, although the potential energy of the system still decreases with the number of geometry updates, the distance between the separated molecules experiences a maximum − they first

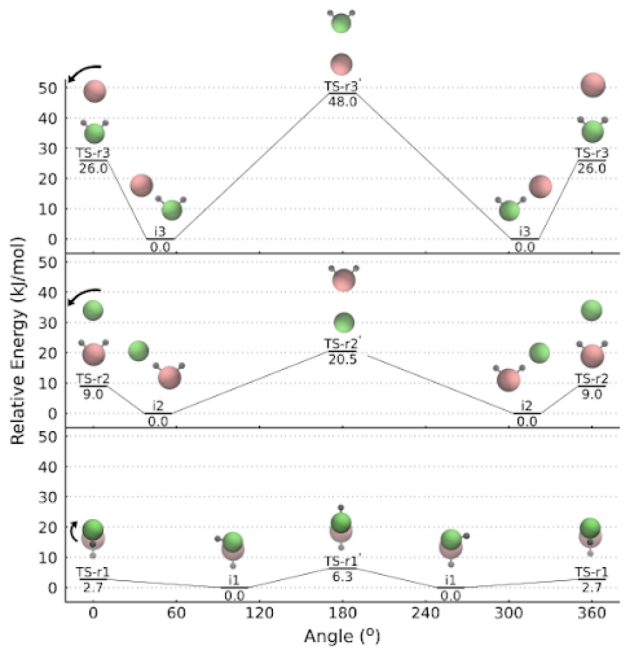

Figure 2. The potential energy profile that is related to **i1** (bottom panel), **i2** (middle panel), and **i3** (top panel). The energy of each panel has been shifted with respect to their corresponding intermediates. ZPE is included, and the color code of the atoms follows Figure 1.

https://doi.org/10.1021/acs.jpca.1c08300
J. Phys. Chem. A 2022, 126, 1465−1474

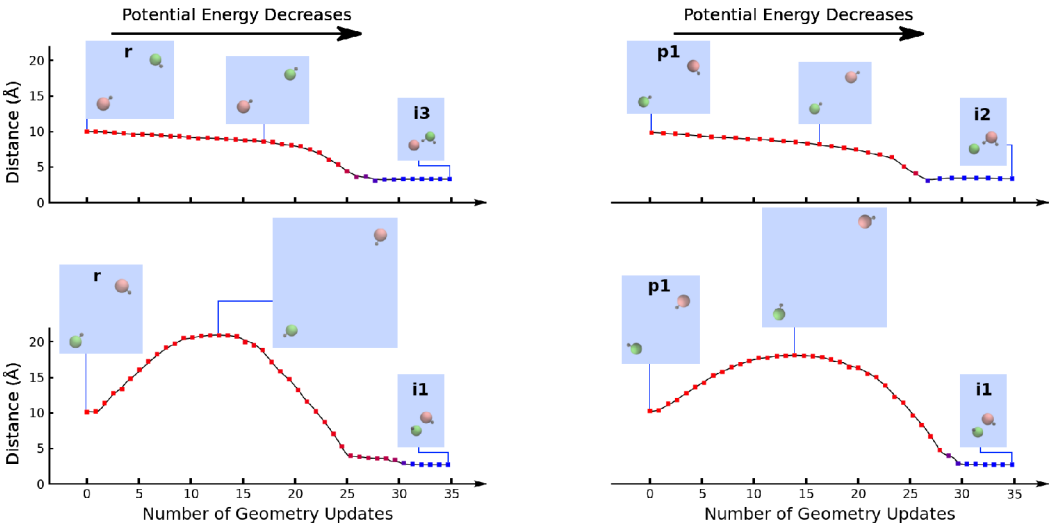

Figure 3. The distance between the geometric centers of the HBr and HCl vs the number of geometry updates. Points are color coded such that warmer colors indicate higher energies. The initial geometry and charges of the separated molecules are prepared similar to **r** (left panel) or **p1** (right panel). The orientation between the separated molecules is prepared similar to **i3** (top left and bottom right panels) or **i2** (top right and bottom left panels). It is important to note that as the points move from left to right, its potential energy decreases.

further dissociate from each other, reorientate, and then associate to form an intermediate that is *different* from the targeted one. As demonstrated in the bottom row of Figure 3, the *distance* between the two reagent molecules experiences a non-neglectable maximum accompanying the geometry update. Eventually, the system converges to **i1** (instead of **i2** and **i3** for the bottom left and bottom right, respectively). As a result, **r**-**i2** and **p1**-**i3** are deemed as having no direct association, and they are not connected in the potential energy profile.

Finally, the geometry of the key points (**i1**, **i2**, and **i3** as well as the TSs connecting them) is analyzed and depicted in Figure S2 in the Supporting Information. As shown, **i1** is largely a van der Waals (vdW) intermediate, with an atomic distance (Br−Cl) of 2.773 Å and a dihedral angle (H−Br−Cl-H) of 97.4°. The rocking motion of the H−Cl/H-Br moiety with respect to Br/Cl leads to formation of **i2**/**i3** by giving up the H. This can be seen by tracking the H−Cl−Br/H−Br−Cl angle which, starting at 97.4/89.8° for **i1**, decreases to 21.3/34.3 for **TS-12**/**TS-13** before eventually vanishing to zero and forming planar **i2**/**i3** intermediates. Since Cl is more electronegative than Br, the latter possesses more net positive charge than the former. Therefore, the rocking motion of H−Br, which results in Cl accepting an additional H (forming **TS-13**), is much easier than the same motion of its counterpart H−Cl (forming **TS-12**). This effect can be seen in the differences in the height of the barriers − **TS-12** (H−Cl rocking) is 107.7 kJ/mol above **i1**, more than double the height of **TS-13** (H−Br rocking).

3.3. Comparison with Similar Bimolecular Collision Systems. The potential energy profile of the bimolecular collision HBr^+ + HCl is compared with reactions of similar sort, namely, the (self) HCl^+ + HCl and HBr^+ + HBr reactions. As stated in section 1, these two reactions have been studied with guided beam experiments and AIMD simulations, and they are reported to respond differently to rotational excitations.[13,14] The most obvious differences between the two self-reactions and the HBr^+ + HCl collisions are the simplification of the potential energy profiles. For example, the **p2** and **p3** in the self-reactions would become one single product, H_2Cl^+ (H_2Br^+) + Cl (Br). In a similar manner, **i2** and **i3** would become one single intermediate in the self-reactions, $[Cl{-}H{-}Cl{-}H]^+$ ($[Br{-}H{-}Br{-}H]^+$), while the counterparts of **i1** (i.e., vdW intermediate) still exist. Another important difference is that the PT/HE product in the self-reactions is thermo-neutral, instead of endothermic in the case of HBr^+ + HCl.

It is of interest to probe into the key structures in detail to analyze the impact of halogens on this reaction. The structures of **i1**'s counterpart, denoted as **i1-Cl** and **i1-Br** for the HCl^+ + HCl and HBr^+ + HBr reactions, respectively, are depicted in Figure 4. As expected, from the perspective of molecular structure, the Cl−Br distance in **i1** is an "average" between those in **i1-Cl** and **i1-Br**. Similar to **i1**, **i1-Cl**/**i1-Br** could also isomerize through the rocking motion of H−Cl/H−Br moiety and form $[Cl{-}H{-}Cl{-}H]^+/[Br{-}H{-}Br{-}H]^+$, denoted as **i2-Cl**

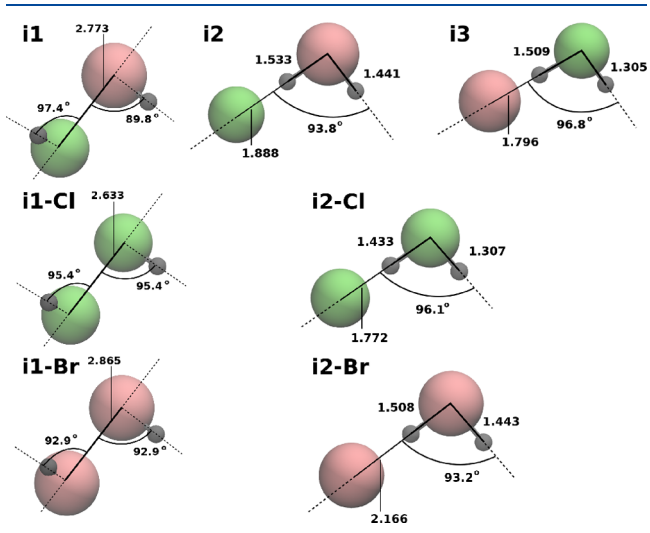

Figure 4. Illustration of **i1**, **i1-Cl**, **i1-Br**, **i2**, **i3**, **i2-Cl**, and **i2-Br** with bond distances (Å) and angles (°). The geometries of **i1-Cl** and **i2-Cl** are reported from Luo et al.[15] while those of **i1-Br** and **i2-Br** are reported from Burda et al.[22]

https://doi.org/10.1021/acs.jpca.1c08300
J. Phys. Chem. A 2022, 126, 1465−1474

Table 1. RMSD (in kJ/mol) of Each Candidate Quantum Chemistry Method Are Computed Using the Equations Above[a]

method	FC-MP2	MP2	B3LYP	BECKE97	BECKE98	PBE0	BNL	rCAM-B3LYP
6-311G**	n/a	n/a	24.9	33.7	25.6	22.1	n/a	n/a
cc-pVTZ	n/a	7.7	25.6	26.0	25.6	23.1	n/a	n/a
def2-SVP	7.2	n/a	29.5	29.2	27.6	26.1	n/a	n/a
def2-SVPD	n/a	7.2	25.3	25.8	38.4	22.4	n/a	n/a
aug-pc-0	30.1	30.9	30.0	34.2	28.7	29.6	28.2	n/a
pc-0	86.8	86.9	90.3	87.0	n/a	88.6	93.9	85.2
def2-TZVP	n/a	14.3	25.8	26.2	24.4	n/a	n/a	n/a
def2-TZVPD	n/a	n/a	24.7	25.6	24.8	22.3	n/a	n/a
LANL2DZ-aug-cc-pVDZ	n/a	21.7	26.5	n/a	n/a	23.2	n/a	13.7
LANL2DZ-cc-pVDZ	23.0	n/a	27.0	n/a	n/a	n/a	10.9	n/a
LANL2DZdp-aug-cc-pVDZ	12.9	12.9	25.7	26.2	24.6	22.5	n/a	n/a
6-31G**	n/a	11.7	28.4	26.4	24.8	36.4	12.6	9.6
LANL2DZdp-cc-pVDZ	13.8	13.3	25.6	n/a	n/a	23.3	11.3	n/a
aug-pc-1	6.5	6.8	24.4	38.6	24.5	22.2	15.3	8.8
aug-pc-2	8.4	8.4	n/a	25.7	24.4	23.5	n/a	n/a
pc-1	n/a	n/a	26.0	26.1	24.9	25.0	13.6	n/a
pc-2	7.9	n/a	25.1	29.3	24.1	21.8	16.8	5.3
Sapporo-DZP-2012	9.6	10.0	25.1	26.0	24.8	23.5	13.9	6.0
Sapporo-DZP-2012-diffuse	54.2	21.3	24.7	n/a	n/a	22.9	n/a	n/a
6-311G*	16.9	16.5	24.6	24.8	25.4	13.4	n/a	n/a
6-31G*	15.7	14.9	25.6	27.1	24.6	14.8	n/a	11.9
aug-cc-pVDZ	n/a	7.0	25.8	25.6	25.5	22.4	14.4	7.3
aug-cc-pVTZ	n/a	10.5	25.2	25.8	24.6	17.5	n/a	n/a
cc-pVDZ	n/a	n/a	26.2	26.6	25.5	n/a	15.8	5.8

[a]The rows list various basis sets and the columns list various computationally efficient methods. "n/a" denotes that for that specific combination of method and basis set, at least one of the key structures could not be optimized after 3000 steps of geometry update.

and **i2-Br**, respectively. There are two interesting comparisons between **i2**/**i3** and **i2-Cl**/**i2-Br**. Once again, shown in Figure 4, the structure of **i2**/**i3** is approximated as an "average" between **i2-Cl** and **i2-Br**. Taking the key character of these structures, the distance (r_{HX}) between the hydrogen bridging between the two halogens and the leaving halogen, as an example, the value of r_{HX} ranks as **i2-Cl** (1.772 Å), **i3** (1.796 Å), **i2** (1.888 Å), and **i2-Br** (2.166 Å) in increasing order. The difference in r_{HX} has a profound effect on the dissociation energy of these compounds as a shorter distance implies a stronger interaction (thus higher dissociation energy). Quite counterintuitively, the highest dissociation energy is found in **i3** (64.6 kJ/mol), followed by **i2-Cl** (53.1 kJ/mo, reported by Luo et al.), **i2-Br** (38.9 kJ/mol, reported by Burda et al.), and **i2** (33.3 kJ/mol). We also note that Burda et al. employed CCSD(T) and reported an even smaller dissociation energy, 31.4 kJ/mol, for **i2-Cl**, but the basis sets (e.g., Christiansen's average relativistic effective pseudopotential)[59] are not as accurate as those used by Luo et al. (e.g., CBS).[25−27] This result suggests that the other halogen (instead of the leaving one) has a non-negligible impact on the dissociation. Another interesting comparison is the barrier between the vdW intermediate **i1** (**i1-Cl** and **i1-Br**) and **i2**/**i3** (**i2-Cl** and **i2-Br**). As discussed in section 3.2, the rocking of HCl moiety of **i1** faces a large energy barrier (**TS-12**, 107.7 kJ/mol above **i1**) before forming **i2**. In comparison, this energy barrier is only 66.6 kJ/mol for **i1-Cl** to isomerize to **i2-Cl**[15] and 79.1 kJ/mol for **i1-Br** to isomerize to **i2-Br**.[22] This difference implies that, should the dynamics of the reaction follow statistical models (e.g., RRKM), there will be less PT/HE products (i.e., **p2** and **p3**) observed in the HBr^+ + HCl reaction compared to the HCl^+ + HCl (i.e., H_2Cl^+ + Cl) and HBr^+ + HBr (i.e., H_2Br^+ + Br) reactions.

3.4. Selecting a Computationally Efficient Method for AIMD Simulations.

The aforementioned mechanism analysis of the HBr^+ + HCl bimolecular collision is based on the potential energy profile and should be examined by dynamics simulations in the future. Fast and accurate calculations of energy gradients are required for these simulations, which in general can be obtained in the following three methods: (1) On-the-fly quantum chemistry calculations: this approach is called AIMD or direct dynamics;[60] (2) a full-dimensional potential energy surface (PES): this approach requires the development of analytical functions (of chemical characteristics) that describe the PES of the system;[61] and (3) a machine-learned PES: this approach is similar to the previous one, but the PES is derived from *ab initio* calculations with machine learning methods and does not necessarily have an analytical expression.[62] Note that the first approach is free of PES development but is limited to the computationally efficient quantum chemistry method due to the number of required energy gradient calculations. This limitation is not as restrictive in the second and third approaches. In this manuscript, a large number of computationally efficient quantum chemistry methods are screened for future AIMD simulation. As stated in section 1, the computationally efficient method suitable for AIMD simulations should accurately represent key structures that are energetically accessible (e.g., all structures in Figure 1, excluding **i4**, **i5**, **TS-24**, **TS-35**, and **p4**). Therefore, the root-mean-square displacement (RMSD) between the benchmark relative potential energy (CCSD(T)/cc-pVDZ//CCSD(T)/CBS) and the potential energy profile computed from a candidate method is measured and employed as a metric to select the computationally efficient method that is closest to the benchmark. It is important to note that the potential energy profile computed from the candidate method

https://doi.org/10.1021/acs.jpca.1c08300
J. Phys. Chem. A 2022, 126, 1465−1474

seeks a maximum overlap with the benchmark, therefore it is subject to shift to minimize the RMSD. The following equations summarize the computation of the RMSD of a candidate method (A) with respect to the reference benchmark (ref):

$$\mathrm{RMSD}(A, \mathrm{ref}) = \sqrt{\frac{1}{K}\sum_{i=1}^{K}\left(E_i^A - E_i^{\mathrm{ref}} - \Delta E(A, \mathrm{ref})\right)^2} \quad (1)$$

$$\Delta E(A, \mathrm{ref}) = \arg\min_{\Delta E}\left(\sum_{i=1}^{K}\left(E_i^A - E_i^{\mathrm{ref}} - \Delta E\right)^2\right) = \overline{E_A} - \overline{E_{\mathrm{ref}}} \quad (2)$$

In the equations above, K is the number of key structures in the benchmark (K = 15 in this study) and $\Delta E(A, \mathrm{ref})$ is the optimal shift in energy between the potential energy profiles of candidate method E_A and the benchmark E_{ref}. The index i denotes the i^{th} structure. $\overline{E_A}$ and $\overline{E_{\mathrm{ref}}}$ are the average relative energy of method A and the benchmark after shifting the energy of the separated reagents (**r** in Figure 1) to zero. The RMSD value of the 192 candidate quantum chemistry methods, that is, 8 computationally efficient methods coupled with 24 different combinations of basis sets and effective core potentials, see section 2.2, are summarized in Table 1.

First of all, it is important to define the purpose of Table 1, which focuses on the performance of these quantum chemistry methods specifically on the key structures related to the collision of HBr^+ + HCl under low excess energy conditions (i.e., <100 kJ/mol, see section 1). Under no circumstances should this table be interpreted as a general comparison of the performance of these methods. We emphasize that the same convergence criteria (the maximum and root-mean-square deviation in energy gradient be $<1.5 \times 10^{-5}$ and 1.0×10^{-5} hartree/Bohr and the maximum and root-mean-square deviation in coordinates to be $<6.0 \times 10^{-5}$ and 4.0×10^{-5} Bohr) are applied to all candidate quantum chemistry methods. The range-separated functionals (BNL and rCAM-B3LYP) show strong basis set dependence − they have problems in identifying one or more key structures with roughly 50% of the tested basis sets. A summary (Table S4) of the number of key structures unidentified for each candidate method is provided in the Supporting Information. Nonetheless, since there have already been numerous combinations of the computationally efficient method and basis sets that are able to identify all the key structures, the focus of the manuscript turns to identify the optimal one for future AIMD study of this reaction.

According to Table 1, traditional DFT functionals like B3LYP, the various Becke functionals, and PBE0 are very robust at identifying all the key structures; however, their respective RMSD values are relatively high (e.g., more than 25 kJ/mol). A closer look at the key structure that had the largest deviation in relative energy from the benchmark reveals that a TS is nearly always (in this case, 138 of the 192 combinations) the largest contributor to the RMSD (see Table S5 in the Supporting Information). This is most certainly an artifact of the fact that those traditional functionals have parametric forms (e.g., for hybrid functionals, the fraction of HF energy) which were empirically fit on stable molecules.[63] The performance of the MP2 and FC-MP2 methods demonstrate very strong basis set dependence, as it has seen some of the smallest RMSD values (e.g., 6.5 kJ/mol, FC-MP2/aug-pc-1; 6.8 kJ/mol, MP2/aug-pc-1) as well as at the same time, some of the largest (e.g., 86.8 kJ/mol, FC-MP2/pc-0; 86.9 kJ/mol, MP2/pc-0). The range separated functionals like BNL and rCAM-B3LYP share similar behavior as the MP2 and FC-MP2, while the overall smallest RMSD is reported from rCAM-B3LYP/pc-2 at 5.3 kJ/mol. It is important to note that this level of agreement of a computationally efficient method is excellent and consequently is as promising as previous, similar AIMD studies in revealing mechanistic details from experimental results (for more details, please see the Supporting Information).[15,36,37,55,56]

The last, but definitely not the least, concern of selecting a candidate method and basis set for AIMD simulations is the computational cost as the number of energy gradient calculations are enormous (see section 2.2). Since the cost of different *ab initio* methods scales differently with the number (N) of basis functions (roughly N^4 for DFTs and N^5 for MP2) and the number of basis functions tested in this study spans a large range (between 26 for LANL2DZ and 155 for aug-cc-pVTZ), the cost of tested candidate methods varies dramatically. As previous AIMD studies have demonstrated, their results are extremely sensitive with respect to the method (e.g., MP2 vs DFT).[64−66] Further, since the computationally efficient method is selected based on optimized structures, while AIMD simulations traverse through unoptimized structure, it is possible that the computationally efficient method with the smallest RMSD performs poorly in AIMD.[15,67,68] Behaviors such as convergence failures, total energy jumps, and/or unphysical charge distributions have been previously reported for AIMD with DFTs.[15,67] Therefore, one DFT functional, the rCAM-B3LYP functional, and one MP2 method, FC-MP2, are recommended. For the former, rCAM-B3LYP functional reports the overall smallest RMSD with pc-2 (5.3 kJ/mol, 105 basis functions), followed by cc-pVDZ (5.8 kJ/mol, 55 basis functions) and Sapporo-DZP-2012 (6.0 kJ/mol, 80 basis functions). For the latter, FC-MP2 reports the smallest RMSD (6.5 kJ/mol) with aug-pc-1, which contains 81 basis functions. As a result, they are selected as candidate methods for future AIMD studies.

4. SUMMARY

This manuscript reports a thorough theoretical investigation of the reaction pathways as a result of the HBr^+ + HCl bimolecular collision. This collision has been exploited by an ion−molecule guided beam to probe the impact of rotational excitation on the dynamics of the reaction, which is more profound when the excess energy is low (e.g., small collision energy, vibrational ground state, etc.). Under such conditions, there are three possible products: HBr + HCl^+, H_2Br^+ + Cl, and H_2Cl^+ + Br. The potential energy profile of key structures (i.e., intermediates and TSs) leading to these products are characterized with high-level *ab initio* calculations, whose validity has been confirmed with experimental results.

This seemingly simple bimolecular system possesses three intermediates, which are connected by a number of low-lying TSs. The dynamics of chemical systems sharing similar characteristics have been reported to experience frequent isomerization and barrier-recrossing. Another interesting feature of the potential energy profile is that each of the intermediates are associated with a self-converting rotational pathway. These rotational pathways could have potential importance to the outcome of the reaction, for example, it provides a means to shuffle the two hydrogens in the systems

https://doi.org/10.1021/acs.jpca.1c08300
J. Phys. Chem. A 2022, 126, 1465−1474

(i.e., Br and Cl end up pairing with different hydrogens than they start with).

These calculations also serve as the benchmark to assess the ability of computationally efficient quantum chemistry method in modeling this reaction in a dynamics simulation. A total of 192 combinations of computationally efficient methods, basis sets, and effective core potentials have been examined, and rCAM-B3LYP/pc-2 and FC-MP2/aug-pc-1 have been identified for their superior accuracy/cost ratio.

■ ASSOCIATED CONTENT

Supporting Information

The Supporting Information is available free of charge at https://pubs.acs.org/doi/10.1021/acs.jpca.1c08300.

Further explanation and summarized results are provided for the benchmarking done in Tables S1−S3 and Figure S1. Comparison of a number of optimized geometries are detailed in Figure S2. Finally, a more detailed overview of the PES deviations used in the RMSD comparison between methods is explained and summarized in Tables S4 and S5 and Figure S3 (PDF)

■ AUTHOR INFORMATION

Corresponding Author

Rui Sun − *Department of Chemistry, University of Hawai'i at Mānoa, Honolulu, Hawaii 96822, United States;* orcid.org/0000-0003-0638-1353; Email: ruisun@hawaii.edu

Authors

Kazuumi Fujioka − *Department of Chemistry, University of Hawai'i at Mānoa, Honolulu, Hawaii 96822, United States*

Karl-Michael Weitzel − *Fachbereich Chemie, Universität Marburg, Marburg D-35032, Germany;* orcid.org/0000-0002-1560-235X

Complete contact information is available at: https://pubs.acs.org/10.1021/acs.jpca.1c08300

Notes

The authors declare no competing financial interest.

■ ACKNOWLEDGMENTS

The authors appreciate the information technology service (ITS) from the University of Hawai'i, Mānoa for the computational resources. The authors are grateful to the financial support from the University of Hawai'i, Mānoa

■ REFERENCES

(1) Polanyi, J. C. Concepts in reaction dynamics. *Acc. Chem. Res.* **1972**, *5*, 161−168.

(2) Moore, C. B.; Smith, I. W. Vibrational-rotational excitation. Chemical reactions of vibrationally excited molecules. *Faraday Discuss. Chem. Soc.* **1979**, *67*, 146−161.

(3) Bradley, K. S. *Theoretical studies of the dynamics of four-atom systems: NH + NO, H + N (2) O, H + CO (2), H + H (2) O, and He + CS (2)*; Ph.D. Dissertation, Northwestern University, 1998.

(4) Sinha, A.; Thoemke, J. D.; Crim, F. F. Controlling bimolecular reactions: Mode and bond selected reaction of water with translationally excited chlorine atoms. *J. Chem. Phys.* **1992**, *96*, 372−376.

(5) Yan, S.; Wu, Y.-T.; Zhang, B.; Yue, X.-F.; Liu, K. Do vibrational excitations of CHD_3 preferentially promote reactivity toward the chlorine atom? *Science* **2007**, *316*, 1723−1726.

(6) Zhang, Z.; Zhou, Y.; Zhang, D. H.; Czako, G.; Bowman, J. M. Theoretical study of the validity of the Polanyi rules for the late-barrier Cl+ CHD_3 reaction. *journal of physical chemistry letters* **2012**, *3*, 3416−3419.

(7) Viggiano, A.; Morris, R. A. Rotational and Vibrational Energy Effects on Ion- Molecule Reactivity as Studied by the VT-SIFDT Technique. *J. Phys. Chem.* **1996**, *100*, 19227−19240.

(8) Xu, Y.; Xiong, B.; Chang, Y. C.; Ng, C. Communication: Rovibrationally selected absolute total cross sections for the reaction H_2O+ ($X\ ^2B_1$; v_1+ v_2+ v_3+= 000; N+ K a+ K c+)+ D_2: Observation of the rotational enhancement effect. *J. Chem. Phys.* **2012**, *137*, 241101.

(9) Ard, S. G.; Li, A.; Martinez, O., Jr; Shuman, N. S.; Viggiano, A. A.; Guo, H. Experimental and theoretical kinetics for the H_2O^++ H_2/D_2 → H_3O^+/H_2DO^++ H/D reactions: Observation of the rotational Effect in the temperature dependence. *J. Phys. Chem. A* **2014**, *118*, 11485−11489.

(10) Papp, P.; Czakó, G. Rotational Mode Specificity in the F^- + CH_3I (v= 0, JK) S_N2 and Proton-Transfer Reactions. *J. Phys. Chem. A* **2020**, *124*, 8943−8948.

(11) Paetow, L.; Unger, F.; Beichel, W.; Frenking, G.; Weitzel, K.-M. Rotational dependence of the proton-transfer reaction HBr^+ + CO_2 → $HOCO^+$ + Br.. I. Energy versus angular momentum effects. *J. Chem. Phys.* **2010**, *132*, 174305.

(12) Paetow, L.; Unger, F.; Beutel, B.; Weitzel, K.-M. Rotational dependence of the proton-transfer reaction HBr^+ + CO_2 → $HOCO^+$ + Br. II. Comparison of HBr^+ ($^2\Pi_{3/2}$) and HBr^+ ($^2\Pi_{1/2}$). *J. Chem. Phys.* **2010**, *133*, 234301.

(13) Uhlemann, T.; Wallauer, J.; Weitzel, K.-M. Self-reactions in the HCl^+(DCl^+)+ HCl system: a state-selective investigation of the role of rotation. *Phys. Chem. Chem. Phys.* **2015**, *17*, 16454−16461.

(14) Schmidt, S.; Plamper, D.; Jekkel, J.; Weitzel, K.-M. Self-Reactions in the HBr^+ (DBr^+)+ HBr System: A State-Selective Investigation of the Role of Rotation. *J. Phys. Chem. A* **2020**, *124*, 8461−8468.

(15) Luo, Y.; Kreuscher, T.; Kang, C.; Hase, W. L.; Weitzel, K.-M.; Sun, R. A chemical dynamics study of the HCl + HCl^+ reaction. *Int. J. Mass Spectrom.* **2021**, *462*, 116515.

(16) Botschwina, P.; Zilch, A.; Rosmus, P.; Werner, H.-J.; Reinsch, E.-A. An abinitio calculation of the near-equilibrium potential energy surface and vibrational frequencies of H2Br+ and its isotopomers. *J. Chem. Phys.* **1986**, *84*, 1683−1686.

(17) Nahler, N. H.; Vieuxmaire, O. P.; Jones, J. R.; Ashfold, M. N.; Eppink, A. T.; Coriou, A. M.; Parker, D. H. High-resolution ion-imaging studies of the photodissociation of the $BrCl^+$ cation. *J. Phys. Chem. A* **2004**, *108*, 8077−8083.

(18) Vieuxmaire, O. P.; Nahler, N. H.; Dixon, R. N.; Ashfold, M. N. Multiphoton dissociation dynamics of BrCl and the $BrCl^+$ cation. *Phys. Chem. Chem. Phys.* **2007**, *9*, 5531−5541.

(19) Wang, M.; Wang, B.; Chen, Z. Theoretical study on potential energy curves and spectroscopy properties of ground and low-lying excited electronic states of $BrCl^+$. *Science in China Series B: Chemistry* **2008**, *51*, 521−528.

(20) Cacace, F.; de Petris, G.; Pepi, F.; Rosi, M.; Sgamellotti, A. Elemental chlorine and chlorine fluoride: Theoretical and experimental proton affinity and the gas phase chemistry of Cl_2H^+ and $FClH^+$ ions. *J. Phys. Chem. A* **1998**, *102*, 10560−10567.

(21) de Petris, G.; Pepi, F.; Rosi, M. Gas-phase reactions of protonated chlorine, Cl_2H^+, with H_2 (D_2) and CH_4. A mass spectrometric and theoretical study. *Chemical physics letters* **1999**, *304*, 191−196.

(22) Burda, J.; Hobza, P.; Zahradník, R. Properties and Reactivity in Groups of the Periodic System: Ion- Molecule Reactions HX+ HX ●$^+$(X= F, Cl, Br, I, At). *J. Phys. Chem. A* **1997**, *101*, 1134−1139.

(23) Raghavachari, K.; Trucks, G. W.; Pople, J. A.; Head-Gordon, M. A fifth-order perturbation comparison of electron correlation theories. *Chem. Phys. Lett.* **1989**, *157*, 479−483.

(24) Dunning, T. H., Jr Gaussian basis sets for use in correlated molecular calculations. I. The atoms boron through neon and hydrogen. *J. Chem. Phys.* **1989**, *90*, 1007−1023.

(25) Helgaker, T.; Klopper, W.; Koch, H.; Noga, J. Basis-set convergence of correlated calculations on water. *J. Chem. Phys.* **1997**, *106*, 9639−9646.
(26) Peterson, K. A.; Dunning, T. H. Benchmark Calculations with Correlated Molecular Wave Functions. 11. Energetics of the Elementary Reactions F+ H_2, O+ H_2, and H '+ HCl. *J. Phys. Chem. A* **1997**, *101*, 6280−6292.
(27) Feller, D. Application of systematic sequences of wave functions to the water dimer. *J. Chem. Phys.* **1992**, *96*, 6104−6114.
(28) Fukui, K. The intrinsic reaction coordinate (IRC) pathway f the chemical reaction. *J. Plays Chem.* **1970**, *74*, 416.
(29) Gonzalez, C.; Schlegel, H. B. An improved algorithm for reaction path following. *J. Chem. Phys.* **1989**, *90*, 2154−2161.
(30) Henkelman, G.; Uberuaga, B.; Jónsson, H. A climbing image NEB method for finding minimum energy paths and saddle points. *J. Chem. Phys.* **2000**, *113*, 9901−9904.
(31) Sheppard, D.; Henkelman, G. Paths to which the nudged elastic band converges. *Journal of computational chemistry* **2011**, *32*, 1769−1771.
(32) Kramida, A.; Ralchenko, Yu.; Reader, J. *Atomic Spectra Database*, ver. 5.8; National Institute of Standards and Technology: Gaithersburg, MD, 2020. https://physics.nist.gov/asd (accessed on June 15, 2021).
(33) Valiev, M.; Bylaska, E.J.; Govind, N.; Kowalski, K.; Straatsma, T.P.; Van Dam, H.J.J.; Wang, D.; Nieplocha, J.; Apra, E.; Windus, T.L.; de Jong, W.A. NWChem: A comprehensive and scalable open-source solution for large scale molecular simulations. *Comput. Phys. Commun.* **2010**, *181*, 1477−1489.
(34) Fedorov, D. G.; Koseki, S.; Schmidt, M. W.; Gordon, M. S. Spin-orbit coupling in molecules: chemistry beyond the adiabatic approximation. *Int. Rev. Phys. Chem.* **2003**, *22*, 551−592.
(35) Fedorov, D. G. Theoretical study of spin-orbit coupling in molecules, Ph.D. Dissertation; Iowa State University, 1999.
(36) Shoji, A.; Schanzenbach, D.; Merrill, R.; Zhang, J.; Yang, L.; Sun, R. Theoretical Study of the Potential Energy Profile of the HBr^+ + CO_2 → $HOCO^+$ + Br· Reaction. *J. Phys. Chem. A* **2019**, *123*, 9791−9799.
(37) Luo, Y.; Fujioka, K.; Shoji, A.; Hase, W. L.; Weitzel, K.-M.; Sun, R. Theoretical study of the dynamics of the HBr^+ + CO_2 → $HOCO^+$ + Br reaction. *J. Phys. Chem. A* **2020**, *124*, 9119−9127.
(38) Sun, R.; Granucci, G.; Paul, A. K.; Siebert, M.; Liang, H. J.; Cheong, G.; Hase, W. L.; Persico, M. Potential energy surfaces for the HBr^+ + CO_2 → Br+ $HOCO^+$ reaction in the $HBr^+{}^2\Pi_{3/2}$ and $^2\Pi_{1/2}$ spin-orbit states. *J. Chem. Phys.* **2015**, *142*, 104302.
(39) Head-Gordon, M.; Pople, J. A.; Frisch, M. J. MP2 energy evaluation by direct methods. *Chemical physics letters* **1988**, *153*, 503−506.
(40) Becke, A. D. A new mixing of Hartree-Fock and local density-functional theories. *J. Chem. Phys.* **1993**, *98*, 1372−1377.
(41) Becke, A. D. Density-functional thermochemistry. V. Systematic optimization of exchange-correlation functionals. *J. Chem. Phys.* **1997**, *107*, 8554−8560.
(42) Schmider, H. L.; Becke, A. D. Optimized density functionals from the extended G2 test set. *J. Chem. Phys.* **1998**, *108*, 9624−9631.
(43) Adamo, C.; Barone, V. Toward reliable density functional methods without adjustable parameters: The PBE0 model. *J. Chem. Phys.* **1999**, *110*, 6158−6170.
(44) Baer, R.; Neuhauser, D. Density functional theory with correct long-range asymptotic behavior. *Physical review letters* **2005**, *94*, 043002.
(45) Yanai, T.; Tew, D. P.; Handy, N. C. A new hybrid exchange-correlation functional using the Coulomb-attenuating method (CAM-B3LYP). *Chemical physics letters* **2004**, *393*, 51−57.
(46) Krishnan, R.; Binkley, J. S.; Seeger, R.; Pople, J. A. Self-consistent molecular orbital methods. XX. A basis set for correlated wave functions. *J. Chem. Phys.* **1980**, *72*, 650−654.
(47) Hariharan, P. C.; Pople, J. A. The influence of polarization functions on molecular orbital hydrogenation energies. *Theoretica chimica acta* **1973**, *28*, 213−222.
(48) Kendall, R. A.; Dunning, T. H., Jr; Harrison, R. J. Electron affinities of the first-row atoms revisited. Systematic basis sets and wave functions. *J. Chem. Phys.* **1992**, *96*, 6796−6806.
(49) Weigend, F.; Ahlrichs, R. Balanced basis sets of split valence, triple zeta valence and quadruple zeta valence quality for H to Rn: Design and assessment of accuracy. *Phys. Chem. Chem. Phys.* **2005**, *7*, 3297−3305.
(50) Rappoport, D.; Furche, F. Property-optimized Gaussian basis sets for molecular response calculations. *J. Chem. Phys.* **2010**, *133*, 134105.
(51) Jensen, F. Polarization consistent basis sets: Principles. *J. Chem. Phys.* **2001**, *115*, 9113−9125.
(52) Noro, T.; Sekiya, M.; Koga, T. Segmented contracted basis sets for atoms H through Xe: Sapporo-(DK)-n ZP sets (n= D, T, Q). *Theor. Chem. Acc.* **2012**, *131*, 1124.
(53) Hay, P. J.; Wadt, W. R. Ab initio effective core potentials for molecular calculations. Potentials for K to Au including the outermost core orbitals. *J. Chem. Phys.* **1985**, *82*, 299−310.
(54) Check, C. E.; Faust, T. O.; Bailey, J. M.; Wright, B. J.; Gilbert, T. M.; Sunderlin, L. S. Addition of polarization and diffuse functions to the LANL2DZ basis set for p-block elements. *J. Phys. Chem. A* **2001**, *105*, 8111−8116.
(55) Manikandan, P.; Zhang, J.; Hase, W. L. Chemical dynamics simulations of X^- + CH_3Y → XCH_3 + Y^- gas-phase S_N2 nucleophilic substitution reactions. Nonstatistical dynamics and nontraditional reaction mechanisms. *J. Phys. Chem. A* **2012**, *116*, 3061−3080.
(56) Paranjothy, M.; Siebert, M. R.; Hase, W. L.; Bachrach, S. M. Mechanism of Thiolate-Disulfide Exchange: Addition-Elimination or Effectively S_N2? Effect of a Shallow Intermediate in Gas-Phase Direct Dynamics Simulations. *J. Phys. Chem. A* **2012**, *116*, 11492−11499.
(57) Ruscic, B.; Pinzon, R. E.; Morton, M. L.; von Laszevski, G.; Bittner, S. J.; Nijsure, S. G.; Amin, K. A.; Minkoff, M.; Wagner, A. F. Introduction to active thermochemical tables: Several "key" enthalpies of formation revisited. *J. Phys. Chem. A* **2004**, *108*, 9979−9997.
(58) Huber, K.-P. *Molecular spectra and molecular structure: IV. Constants of diatomic molecules*; Springer Science & Business Media: New York, 2013.
(59) Fernandez Pacios, L.; Christiansen, P. A. Ab initio relativistic effective potentials with spin-orbit operators. I. Li through Ar. *J. Chem. Phys.* **1985**, *82*, 2664−2671.
(60) Pratihar, S.; Ma, X.; Homayoon, Z.; Barnes, G. L.; Hase, W. L. Direct chemical dynamics simulations. *J. Am. Chem. Soc.* **2017**, *139*, 3570−3590.
(61) Li, J.; Zhao, B.; Xie, D.; Guo, H. Advances and new challenges to bimolecular reaction dynamics theory. *J. Phys. Chem. Lett.* **2020**, *11*, 8844−8860.
(62) Noé, F.; Tkatchenko, A.; Müller, K.-R.; Clementi, C. Machine learning for molecular simulation. *Annu. Rev. Phys. Chem.* **2020**, *71*, 361−390.
(63) Lynch, B. J.; Truhlar, D. G. How well can hybrid density functional methods predict transition state geometries and barrier heights? *J. Phys. Chem. A* **2001**, *105*, 2936−2941.
(64) Mikosch, J.; Zhang, J.; Trippel, S.; Eichhorn, C.; Otto, R.; Sun, R.; de Jong, W. A.; Weidemuller, M.; Hase, W. L.; Wester, R. Indirect dynamics in a highly exoergic substitution reaction. *J. Am. Chem. Soc.* **2013**, *135*, 4250−4259.
(65) Sun, R.; Davda, C. J.; Zhang, J.; Hase, W. L. Comparison of direct dynamics simulations with different electronic structure methods. F^- + CH_3I with MP2 and DFT/B97−1. *Phys. Chem. Chem. Phys.* **2015**, *17*, 2589−2597.
(66) Zhang, J.; Lourderaj, U.; Sun, R.; Mikosch, J.; Wester, R.; Hase, W. L. Simulation studies of the Cl^- + CH_3I S_N2 nucleophilic substitution reaction: comparison with ion imaging experiments. *J. Chem. Phys.* **2013**, *138*, 114309.
(67) He, C.; Fujioka, K.; Nikolayev, A. A.; Zhao, L.; Doddipatla, S.; Azyazov, V. N.; Mebel, A. M.; Sun, R.; Kaiser, R. I. A chemical dynamics study of the reaction of the methylidyne radical (CH, X $^2\Pi$) with dimethylacetylene (CH_3CCCH_3, X $^1A_{1g}$). *Phys. Chem. Chem. Phys.* **2021**, *24*, 578−593.

https://doi.org/10.1021/acs.jpca.1c08300
J. Phys. Chem. A 2022, 126, 1465−1474

(68) Doddipatla, S.; He, C.; Kaiser, R. I.; Luo, Y.; Sun, R.; Galimova, G. R.; Mebel, A. M.; Millar, T. J. A chemical dynamics study on the gas phase formation of thioformaldehyde (H_2CS) and its thiohydroxycarbene isomer (HCSH). *Proc. Natl. Acad. Sci. U. S. A.* **2020**, *117*, 22712−22719.

https://doi.org/10.1021/acs.jpca.1c08300
J. Phys. Chem. A 2022, 126, 1465−1474